

OMAE2008-57073

ON INFLUENCE OF TURBULENCE MODELLING ON CAVITATION PREDICTION FOR FLOW AROUND P1356 SHIP PROPELLER

Conxita Lifante
CFX Development
ANSYS Germany GmbH
Otterfing
Germany

Thomas Frank
CFX Development
ANSYS Germany GmbH
Otterfing
Germany

Karsten Rieck
Schiffsbau-Versuchsanstalt
Potsdam GmbH
Potsdam
Germany

ABSTRACT

The goal of this work is to get a deeper understanding of the structure of the flow around a propeller of a passenger ship, specially the pressure field, where turbulent fluctuations and cavitation can lead to pressure oscillations, vibration and noise. The accurate prediction of cavitation has been found out to be intrinsically related to the accurate resolution of turbulent structures of the flow. Therefore, a thoroughly analysis of the turbulence modeling in this kind of application was performed.

Following the Best Practice Guidelines (BPG) [1] different grids and turbulence models have been investigated. The numerical results obtained have been compared to the experimental data generated at SVA Potsdam, which includes transient pressure signals as well as cavitation patterns. A highly satisfactory agreement between numerical solutions and experiments is observed for the finest grids and a scale-resolving turbulence modeling approach (DES/SAS).

KEY WORDS: cavitation, turbulence, DES, marine applications.

INTRODUCTION

Cavitation in marine applications like flows around ships and propellers is a phenomenon, which can lead to serious performance deterioration of propellers, to damages to their blades and to loss of comfort due to the induced pressure fluctuations. Therefore large efforts are spent into the investigation of cavitation inception and accurate prediction of cavitation for existing and new marine technology designs. Due to high operational costs of experimental investigations it is highly desirable to be able to study cavitation with reliable CFD techniques. The aim of this work is to investigate

cavitation occurring at the propeller blades of a P1356 passenger ship. Experimental data provided by the Schiffsbau-Versuchsanstalt Potsdam GmbH (SVA) are used to validate the numerical simulations performed using ANSYS CFX. Among other facilities, SVA operates a towing tank and a cavitation tunnel. In the cavitation tunnel the P1356 propeller model was investigated with a plate located 18.2cm above the propeller and four pressure transducer probes on the plate. The plate with pressure transducers is representing the very simplified ship stern and the pressure sensors were used to record transient pressure signals in order to study the propeller/ship stern interaction in cavitating and not cavitating flow conditions.

Grid and turbulence modeling dependencies are found to play a crucial role in order to reproduce accurately the pressure field around the propeller, and furthermore in accurate prediction of vortex induced cavitation.

Previous work of the authors [2][3][4] revealed the strong influence of the turbulence modeling on cavitation prediction, especially in the case of turbulence induced cavitation due to formation of recirculation zones or departing tip vortices. In case of the numerical simulation of flows around hydrofoils with tip vortex cavitation it was observed, that a more accurate turbulence modeling lead to a substantially improved resolution of the steep gradients in circumferential velocities in the regions of departing tip vortices and consequently in an improved prediction of turbulence induced local pressure minima, which in turn can lead to inception of local cavitation.

Different approaches are considered for the generation of the grid (by means of the ICEM CFD software) not only including regular spatial refinement but also the adequate location of nodes in the more essential zones of tip vortex cavitation by applying locally unstructured meshing techniques

to selected blocks of a structured mesh in combination with a new technique for the rotor-stator interface around the propeller. Specially demanding is the resolution of the grid in locations, where the tip vortices depart from the blade tips of the propeller. Trailing vortices from blade tips represent comparable small spatial structures and their sufficient resolution in space is essential for the vortex representation in the CFD solution and for small numerical diffusion to the large pressure and velocity gradients in these vortex structures. The exact as possible prediction of the local pressure minima in the tip vortex cores is finally of essential importance for the prediction of vortex induced cavitation inception in these numerical simulations.

Different turbulence models are analyzed and compared to each other, starting from a transient two-equation approach by means of the SST model, EARSM, a $k-\omega$ -based RSM (turbulence viscosity based URANS methods) and ending up with scale-adaptive simulation (SAS) or DES computations. The numerical results obtained show satisfactory agreement to the experimental data, and the use of ANSYS CFX has proven to be an accurate and suitable tool to investigate the phenomena of tip vortex separation and cavitation inception on propeller blades in marine applications.

TEST CASE DESCRIPTION

The test case analyzed is the flow around a passenger ship propeller called P1356. It has been investigated experimentally as well as numerically. Experiments were performed in the cavitation tunnel operated at SVA, where the propeller has been investigated under open water conditions (uniform inflow). And the experimental data obtained were afterwards used to validate the numerical simulations performed by using the ANSYS CFX software package.

The propeller consists of 5 blades and has a diameter of $D=0.25$ m. The specific configuration presented here consists of a rotation frequency of $n=28$ s^{-1} , a propulsion coefficient of $J=0.6$ and the cavitation number of $\sigma_n=1.816$.

The propeller has been investigated inside the cavitation tunnel with a transducer plate located 18 cm above the propeller, where 4 different probes were arranged in a regular pattern on the surface of the plate in order to record transient pressure values at pressure sensor locations. The pressure transducer plate is used in this arrangement as a strongly simplified replacement of a real ship stern model in order to study the propeller/ship hull interaction by propeller and cavitation induced pressure fluctuations. Recorded transient pressure signals are then used for the validation of CFD simulation results. Therefore the same propeller configuration and geometry at the same scale was used for the numerical simulations. A schematic representation of the propeller, the pressure transducer plate arrangement and the probe distribution is shown in Figure 1.

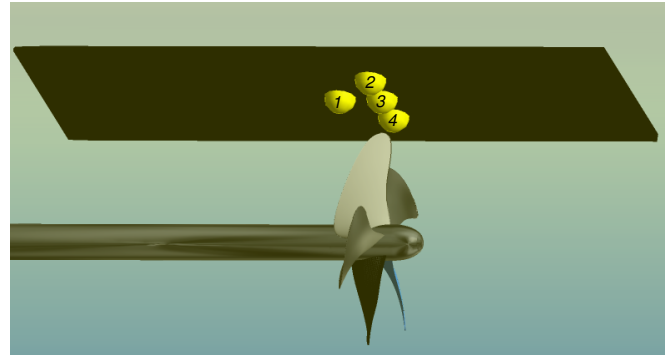


Figure 1: Test case configuration: propeller, transducer plate and probe locations.

The inner cross section of the SVA Potsdam cavitation tunnel is 850×850 mm^2 , its maximum flow velocity is 7.5 m/s, the maximum measurable thrust with the used dynamometer is 3000 N and the maximum measurable torque is 150 Nm.

The experimental data were generated after the propeller was rotating for long time, therefore assuring the independency of the recorded data from cavitation tunnel initial state. Then the signal corresponding to 10 cycles was recorded by using Stereo PIV measurements [5]. The camera used has a sensor resolution of 1024×1024 pixels, and it can take from 60 to 2000 Pictures/second using the highest resolution and up to 120000 Pictures/second using the lowest one. The resolution chosen for this case was 6000 Pictures/second containing 512×512 pixels each one.

Regarding the pressure data, transient signals have been recorded with miniaturized pressure sensors of XPM5 type with an adjustable range of measurement between 0-2 bar up to 0-350 bar [6]. For higher reliability of data, clearer plot representation and comparison to CFD results, a statistical average of the data over 10 propeller cycles was obtained.

NUMERICAL SIMULATIONS

As mentioned before, the work has been focused on two main aspects due to their great influence on the accuracy of the numerical results, and therefore the cavitation prediction. These are the grid resolution, taking special care about the spatial mesh resolution of the zone behind the propeller where tip vortices are expected to occur; and the modeling of the fluid turbulence.

Numerical Meshes

The domain has been discretized using the mesh generator ANSYS ICEM-CFD [7] It has been split into two parts: one containing the area around the propeller blades (rotating region), and another one for the remaining static part of the domain. This is due to the fact that ANSYS CFX [8] allows running different zones of the domain with either rotor or static

frame of reference, and connecting them by using so-called general grid interfaces (GGI) at the rotor/stator interfaces.

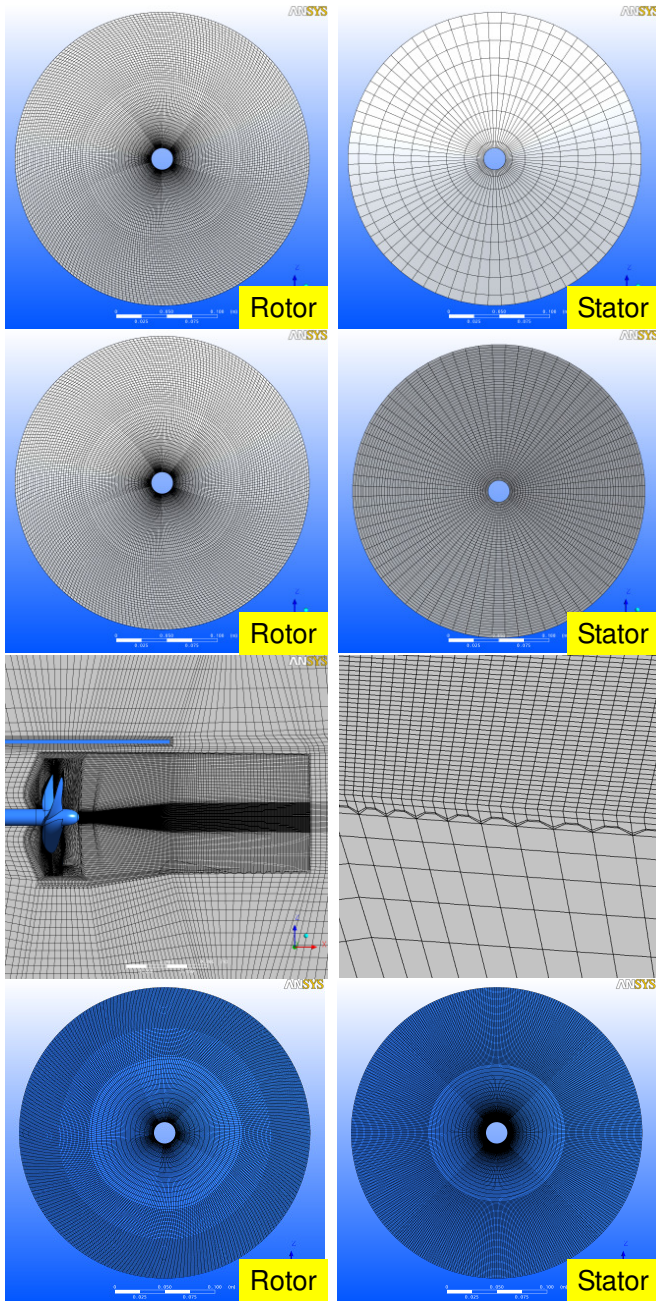


Figure 2: Grid resolution details for different meshes. From top to bottom: Grid 1 (rotor/stator interface); Grid 2 (rotor/stator interface), Grid 3 (structured/unstructured grid coarsening); Grid 5 (rotor/stator interface).

In this way the propeller and a small part of the hub have been simulated in a rotor frame, while the rest of the domain (including the transducer plate) has been simulated in a static

frame. As will be explained next, the spatial resolution of the grid at the interface between those two parts plays an important role in order to assure high accuracy of the numerical solutions.

Five different consequently refined grids were investigated (see Figure 2).

The first approach (Grid1) contained about 1.4 Mio nodes in total. Due to the skewness of the propeller blades the minimum grid angle was about 9.25 degrees. Due to the generation of a scalable grid structure, this minimum grid angle could be preserved throughout the following steps of grid refinement, thereby assuring a constant mesh quality for all CFD predictions. The grid resolution at the rotor/stator interface in both domains was pointed out to be of quite significant influence on the CFD simulation results.

Therefore, the second step (Grid 2) consisted of refining the stator in order to get a more similar spatial resolution on both sides of the interface. Even with this approach the grid resolution of the static part of the computational domain was still rather coarse. Refining the grid at the stator domain in order to reach the same resolution as at the rotor side of the rotor/stator interface would imply a propagation of the refinement through the whole stator domain ending up with an enormous amount of nodes and consequently with a much too high computational effort for the computational flow prediction.

Therefore the third grid (Grid3) avoids this grid refinement propagation by applying a new feature of the ANSYS ICEM-CFD grid generator [9]. It allows generating a non-structured layer that creates a smooth transition between a densely refined zone of the grid and a coarser one (Figure 2). This way only a minor part of the stator (the one just after the interface, where the system of tip vortices is propagating downstream of the propeller) is refined, resulting in a similar spatial resolution on both sides of the rotor/stator interface.

The fourth mesh uses the same meshing strategy but nodes in the refined part of the stator domain are more concentrated in the area where the tip vortices departing from the blades are supposed to propagate. The final grid (Grid5) is a refinement of the previous one including an extension of the zone right after the interface where the grid is refined. The main characteristics of the grids used for the numerical simulations are summarized in Table 1.

	Nodes at rotor domain	Nodes at stator domain	Min grid angle
Grid1	1.159.050	270.460	9.25°
Grid2	1.159.050	605.620	9.25°
Grid3	1.159.050	3.117.222	9.25°
Grid4	1.196.825	3.847.814	9.00°
Grid5	1.627.550	8.464.877	9.90°

Table 1: Grid statistics

Numerical Setup and Turbulence Modeling

The simulations presented in this work have been run in a transient mode using a single-phase CFD setup with water under normal conditions as the working fluid. A high resolution numerical scheme has been chosen for the advection term and a second order backward Euler scheme for the transient term.

The following boundary conditions were applied to solve the test case:

- Inlet boundary condition with an inlet velocity value (uniform inflow) based on the advance coefficient and rotation frequency.

$$v_{in} = JnD \quad (1)$$

- Outlet boundary condition with a static outlet pressure based on the cavitation number.

$$p_{out} = p_v + \sigma_n \left(\frac{\rho}{2} n^2 D^2 \right) \quad (2)$$

- No-slip wall boundary condition for the cavitation tunnel walls and the solids inside the domain.

Different turbulent methods were investigated: the standard SST formulation; SST including a curvature correction to take into account the strong swirl present in the flow at the location of tip vortices; the Explicit Algebraic Reynolds Stress Model (EARSM); the $k-\omega$ based Baseline Reynolds Stress Model, where an equation is solved for each of the 6 independent tensor components of the Reynolds stress tensor; and finally the Scale Adaptive Simulation (SAS) model.

In all cases an automatic wall treatment method is applied, which automatically switches from wall-functions to a low-Re formulation as the mesh is refined.

Most of the flows that can be observed in nature or engineering processes are turbulent. It is due to the fact that they are three dimensional flows, unsteady and may contain many different length scales, originating a complex process. The Navier-Stokes equations are still valid for turbulent flows. However, turbulent flows span the range of length and time scales involving scales much smaller than the smallest finite volume size. The computing power required for the Direct Numerical Simulation (DNS) of this kind of flows is further beyond the available one, particularly in cases of industrial interest. Major effort has been carried out by the scientific community in order to take into account the turbulent effects on the flow. Different approaches can be applied such as resolving the large-scale turbulent fluctuations containing the major part of the turbulent kinetic energy (LES, DES, SAS) or

modelling the phenomena entirely. When attempting to model the turbulence, turbulence viscosity models can be applied. The turbulence or eddy viscosity models are statistical models and consider that the main variables are compound by an average component and an additional time-varying fluctuating one, like

$$u_i = \bar{u}_i + u_i' \quad (3)$$

Introducing this decomposition into the Navier-Stokes equations (1-2) and time-averaging them, the so-called Reynolds Averaged Navier-Stokes (RANS) equations are obtained

$$\begin{aligned} \frac{\partial(\rho_m \bar{u}_i)}{\partial t} + \frac{\partial(\rho_m \bar{u}_i \bar{u}_j)}{\partial x_j} = \frac{\partial \bar{P}}{\partial x_i} + \rho_m g_i + \\ + \frac{\partial}{\partial x_j} (\bar{\tau}_{ij} - \rho_m \overline{u_i' u_j'}) + S_{M_i} \end{aligned} \quad (4)$$

Simulations using the RANS equations substantially reduce the computational effort in comparison with DNS and it is generally adopted for engineering applications. However, the averaging procedure introduces additional unknown terms containing products of the fluctuating components, which act like additional stresses in the fluid. These stresses are difficult to determine directly and must be modelled by means of additional equations or quantities in order to close the set of equations. Eddy viscosity models assume that the Reynolds stresses can be related to the mean velocity gradients and turbulent viscosity by the gradient diffusion hypothesis in an analogous manner to Newtonian laminar flow as:

$$\begin{aligned} \overline{\rho_m u_i' u_j'} = \frac{2}{3} \rho_m k \delta_{ij} + \frac{2}{3} \mu_t \frac{\partial}{\partial x_i} \bar{u}_j \delta_{ij} \\ - \mu_t \left(\frac{\partial}{\partial x_j} \bar{u}_i + \frac{\partial}{\partial x_i} \bar{u}_j \right) \end{aligned} \quad (5)$$

where μ_t is the eddy viscosity or turbulent viscosity, and needs to be evaluated.

A two-equation turbulence model represents a good compromise between numerical effort and computational accuracy. Two extra transport equations must be solved ($k-\epsilon$, or $k-\omega$). The turbulent viscosity is modelled as the product of a turbulent velocity and a turbulent length scale. The turbulent velocity scale is computed from the turbulent kinetic energy (k), and the turbulent length scale is estimated from either the turbulence kinetic dissipation rate (ϵ) or the turbulence frequency (ω).

A representative of the two-equation models is the SST (Shear Stress Transport) turbulence model. The SST model 00 is based on the combination of two underlying two-equation turbulence models, the industrially wide-spread $k-\epsilon$ -model (Jones and Launder, 0), and the $k-\omega$ model in the formulation of Wilcox 00. The hybrid procedure consists of the k -equation and a special form of the ω -equation, which enables through changing the value of a blend factor switching between a ω -equation and a ϵ -equation.

In order to correct for the effects of the streamline curvature or rotation of the overall system, corrections to the turbulence model were introduced. One of them was suggested by Spalart and Shur 0, based on the thickness of the eddy. A factor introducing a correction of the turbulence size is included. Applied to the formulation of the SST model, this results in the correction term in the formulation by Langtry and Menter 0 as chosen in these investigations for the SST model with curvature correction.

When the stress tensor components must be computed more accurately or the underlying assumption of isotropic turbulence is violated, Reynolds Stress Models can be applied. They are based on transport equations for all independent components of the Reynolds stress tensor and the dissipation rate (or the turbulence frequency). Algebraic Reynolds Stress models solve algebraic equations for each individual component of the tensor, while differential methods solve a differential transport equation. In this case the computational effort is consequently increased. In addition to the EARSM a ω -based Reynolds Stress model was chosen for the present work: the so-called BSL Reynolds stress model.

Again the model blends from a ω -based model to a ϵ -based model. The blending is done by means of a smooth linear interpolation in a similar way as for the SST method 0.

In addition to the turbulence viscosity models, another family of methods can be used known as Large Eddy Simulation (LES), consisting of filtering the Navier-Stokes equations and the decomposition of the flow variables into large resolved scales and small or sub-grid scales, which have to be modelled. However, this technique is computationally very expensive when it is applied to industrial problems. In this context arises the need of the use of Scale-Adaptive Simulations (SAS). It is an improved URANS formulation, which allows the resolution of the turbulent spectrum in unstable flow conditions. The SAS method 0 is based on the Von Karman length scale. Depending on it, the model adjusts to a URANS simulation, with LES-like behaviour in unsteady regions, or to RANS simulation in stable flow regions or in regions with a non-sufficient spatial resolution of the underlying mesh in order to resolve the turbulent scales and structures, e.g. in the far field of the flow around a blunt body.

As it will be shown in next section, it was found that the use of either a turbulence modelling scheme or another plays an important role in the simulation. Amongst the statistical turbulence models based on the turbulence viscosity hypothesis, the applied differential Reynolds Stress Model

(BSL RSM) lead to more accurate predictions of the rotational velocity (which presents a steep profile) in case of tip vortex cavitation than SST computations.

RESULTS

Two main characteristics or target properties have been analyzed in order to evaluate the results obtained with respect to the different grids and different turbulence models, which are the transient, ensemble averaged pressure signals at the probes located on the transducer plate and the tip vortex structure of the flow departing off the tips of the propeller blades and propagating downstream the cavitation tunnel behind the propeller. The first ones can be compared to recorded pressure data from the CFD simulations (Figure 3, Figure 4, Figure 5), while the second ones can be compared to visual observations and movies obtained directly from high-speed camera at the cavitation tunnel at SVA (Figure 6, Figure 7).

Test name	Grid	Turbulence Model
1A	1	SST
1B	1	SST+CC
1C	1	BSL-RSM
2A	2	SST
2B	2	SST+CC
2C	2	BSL-RSM
2D	2	EARSM
3A	3	SST
3B	3	SST+CC
3C	3	BSL-RSM
3D	3	EARSM
3E	3	SAS-SST
4E	4	SAS-SST
4F	4	DES
5F	5	DES

Table 2: Test cases investigated.

Simulations Outline

In order to investigate the influence of the two parameters (grid resolution, and turbulence modeling) different configurations were analyzed. Their description is summarized in Table 2. Besides the application of turbulence viscosity based URANS models, for the sufficiently refined numerical grids 3-5 also scale-resolving turbulence modeling (SAS-SST and DES) has been applied in the numerical simulations in order to reproduce the flow structure of detaching tip vortices correctly.

Transient Pressure Signals

The influence of the turbulence modeling can be observed in Figure 3. On its top, the transient pressure signal at the probe number 2 for the 1A/1B/1C configurations is shown. Results show that for the Baseline Reynolds Stress Model approach the phase and the amplitude of the pressure signal is in better agreement with the experimental data than for the case using the standard SST w/o curvature correction, as could be expected, since it represents the more accurate turbulence model.

The middle graphic contains the transient pressure signal for the 2B/2C/2D configurations. In this case, the phase and amplitude prediction of the pressure signal is similar for the different models. There is no shift on the phase of the profiles, and the EARSM and the BSL-RSM show a very similar performance.

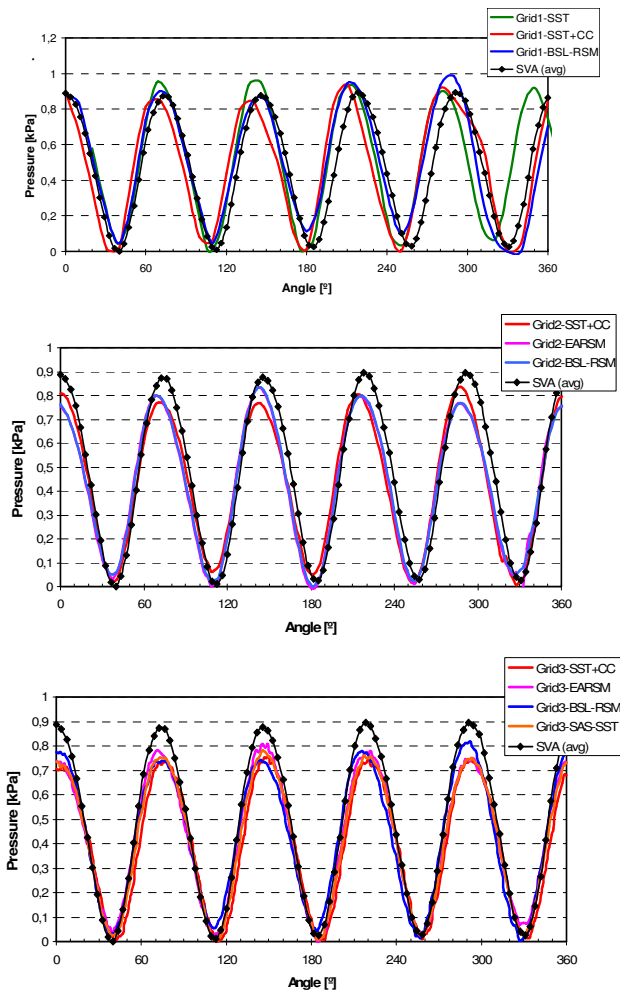


Figure 3: Transient pressure signal at probe 2 for different turbulence models.
Top: Grid 1; Middle: Grid 2; Bottom: Grid 3.

Results on the bottom correspond to the 3B/3C/3D/3E simulations. The same qualitatively behavior can be observed. The influence of the grid resolution can be noticed in Figure 4. Results for the second probe, in this case for the simulations 3E/4F/5F, are compared again to the experimental data. No significant difference between the fourth grid results and the third grid results is observed, as expected since the number of grid nodes is of the same order, grid resolution of the rotor domain is the same and only the location and number of nodes inside the rotor domain is changed. However, when the results on the 8.5 Mio nodes grid are analyzed (grid 5), it can be seen that the CFD simulations predict highly satisfactory the experimental results, even reaching the same amplitude level. The last grid contains more than twice the amount of nodes than the previous one.

For the sake of brevity not all results corresponding to the other three probes are included. The qualitative results are the same, and the same trends were observed. Just the results for the case 5F (Grid 5, solved with the DES turbulence model), are shown (Figure 5).

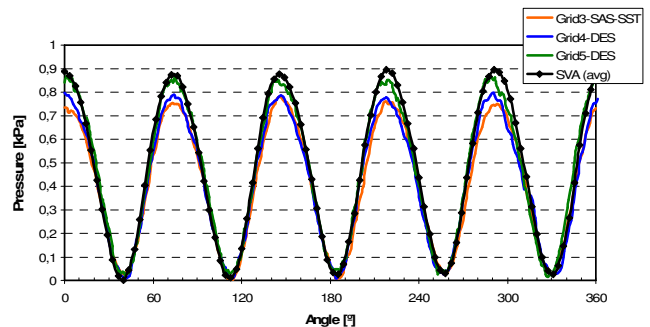
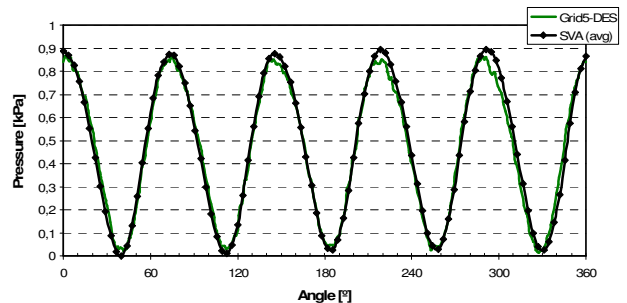


Figure 4: Transient pressure signal at probe 2 . Case 3E, 4F, 5F.

The transient pressure signals at the second and fourth probe are in good agreement with the experimental data, and only for the third one the discrepancies are larger.



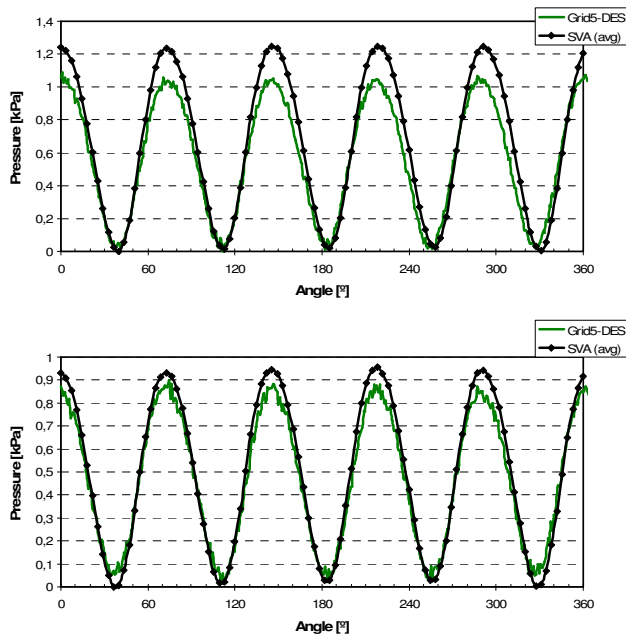


Figure 5: Transient pressure signal. Case 5F. Top: probe 2; Center: probe 3; Bottom: probe 4.

The accurate prediction of the pressure field leads in turn to an accurate prediction of local pressure oscillations and the formation of cavitating zones due to locally decreasing pressure below the saturation pressure of the fluid. It was found that it was necessary to use the finest grid and more accurate scale-resolving turbulence model to reproduce the experimental values. However, by comparing only the transient pressure signal, it could be thought that the difference between, for instance, grid 3 and 4 is not of large importance. Pictures presented in next section show, that besides the achieved accuracy of the transient pressure signals special effort has to be undertaken in order to reproduce the details of the flow structure behind the propeller.

Prediction of Tip Vortex Structure

Since the final goal of the presented CFD study is the prediction of cavitation and the locations at the propeller blade surfaces where this will take place, the structure of the flow was investigated. Flow and vortex structure was analyzed more thoroughly by visualization of isosurfaces of the pressure field and turbulence related quantities.

In Figure 6 pressure isosurfaces for the five analyzed grids are plotted. Results correspond to the most accurate turbulence model in each case, so BSL RSM for grids 1-3 and DES for grids 4-5. The visualized domain includes the rotor including the propeller blades and the area in downstream direction. Black lines on the pictures represent the discretization of the rotor/stator interface from the rotor point of view.

It was clearly found, that the first grid contained a too significant different resolution on both sides of the rotor/stator interface. Therefore a significant amount of information was lost at the rotor/stator interface due to interpolation errors. This can be noted because the tip vortices departing from the blades suddenly disappear on the interface location. The diffusion due to the interpolation between rotating and static parts of the computational domain does not allow them to cross the interface.

The second grid was refined in the circumferential direction in order to get a more similar spatial resolution on the mentioned interface. A slight improvement could be observed, because now the tip vortices cross the interface, but only a very short distance, almost insignificant. This indicated that the refinement was not still not sufficiently high, especially on the stator part of the domain adjacent downstream of the rotor domain. Thus, the necessity of a new meshing strategy arose.

The third grid simulation shows a notable progress in this sense. The isosurface length is larger, crossing the interface without losing information. However, it looked not long enough as in the experimental facilities. In this case an optimization of the local node density was required, which was achieved by reallocation of nodes to the region, where the tip vortices propagate from the rotor domain into the stator domain keeping the overall number of nodes on the mesh almost constant.

The numerical results obtained with the fourth grid are more adequate in terms of tip vortices length prediction. The issue at the interface is totally fixed, and the characteristics of the results depend now on the global mesh parameters. However, some non-physical gaps in the lateral vortex structures appeared. This effect was not due to any deficiencies of the physical modeling but is related to the fact of non-appropriate projections of the edges of grid blocks in the far field behind the propeller. Larger cell sizes in the corners of rectangular grid block structures lead to a local coarsening of the numerical mesh with increasing distance to the rotor of the propeller and therefore to a deterioration in spatial resolution, which caused the tip vortices to disappear locally.

By fixing this meshing issue in grid 5 and by enlarging the area just behind the rotor/stator interface where the grid is refined, a very satisfactory result in agreement with the experimental observations was achieved. The pressure isosurfaces visualizing the location of the tip vortices show now a very comparable shape in comparison to the cavitation tunnel observations.

Since the resolution of the cavitation has an intrinsic relation with the degree of turbulence resolution, turbulence quantities can help us for the study and visualization of the flow structure. In this way, the so called Q-criteria value was analyzed. It is a velocity gradient invariant considering the vorticity and shear strain rate of the flow. It can be mathematically described as

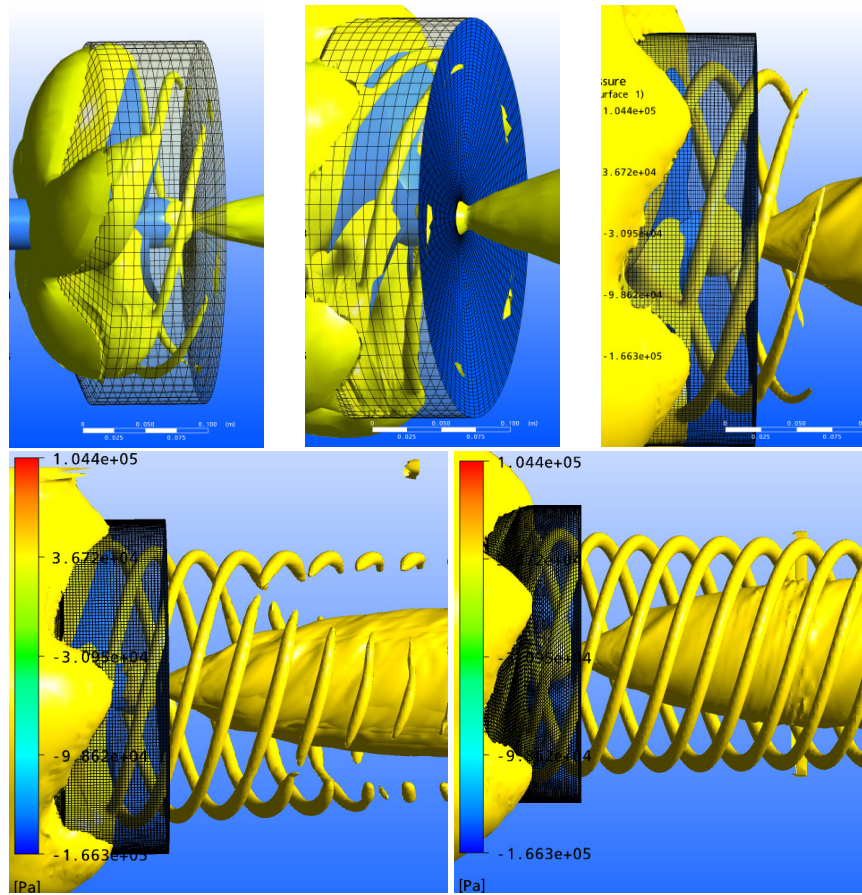


Figure 6: Pressure isosurface ($P=47\text{KPa}$) for the different grids. Top left: Case 1C; Top middle: Case 2D; Top right: 3F; Bottom left: Case 4F; Bottom right: Case 5F.

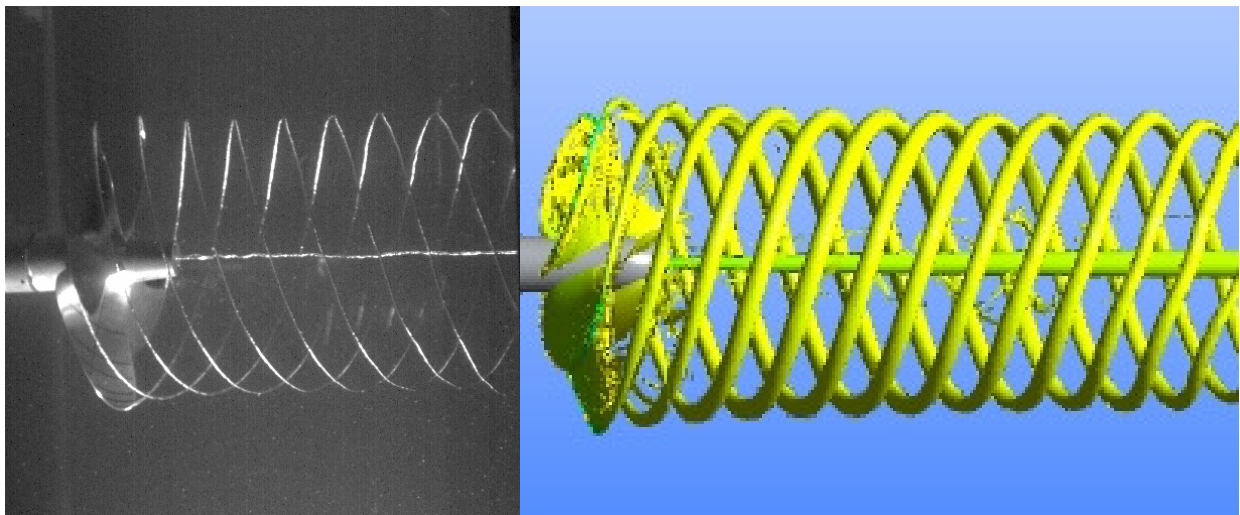


Figure 7: Left: Propeller at the cavitation tunnel at SVA; Right: Q -criteria isosurface obtained with numerical simulation, case 5F ($Q=50$).

$$Q = \Omega^2 - S^2 = \left(\frac{\partial u_i}{\partial x_j} - \frac{\partial u_j}{\partial x_i} \right)^2 - \left(\frac{\partial u_i}{\partial x_j} + \frac{\partial u_j}{\partial x_i} \right)^2 \quad (6)$$

This value has units of [s⁻²]. In order to deal with a dimensionless parameter a modification of it was used. It has been done considering one of the more significant values characterizing the configuration of the flow, which is the rotation frequency of the propeller (n).

$$Q^* = Q/n^2 \quad (7)$$

In there is a qualitatively comparison between a snapshot of the cavitation tunnel while the propeller is rotating (left) with the same parameters defined in the numerical simulations, and a plot of a Q^* -criteria isosurface obtained with the finest grid and DES model. It can be noted that the degree of agreement is fully satisfactory in terms of predicted flow structure behind the propeller.

CONCLUSIONS

The study of a flow around a ship propeller by means of CFD simulations was presented. This kind of flows are of large interest for the marine industry, and usually very costly when analyzed experimentally.

The main focus of the investigations was two-fold: to study the influence of grid resolution and turbulence modeling on transient pressure oscillations caused by the propeller flow and on the flow structure downstream of the propeller.

Therefore, different grids and turbulence models were considered. Both of them were found to have an important influence on the accuracy of the numerical solution, especially with respect to the spatial and timely resolution and downstream propagation of tip vortex structures departing from blade tips of the propeller.

Numerical results were compared to experimental data obtained from scaled model experiments at SVA Potsdam test facilities. With the finest grid and by applying a scale-resolving DES turbulence model very satisfactory agreement between numerical predictions and experiments could be observed, in terms of transient pressure signal predictions at given measurement locations and in terms of the predicted and visually observed flow structure behind the propeller blades.

The information obtained from the presented and discussed single-phase simulations indicate, that a multiphase simulation applying a cavitation model would require even finer grids in order to resolve the small geometrical structures of tip vortices and consequently the drop of the local pressure in tip vortices below the saturation pressure, which finally

would lead to the tip vortex cavitation observable in the experiments.

NOMENCLATURE

D	Propeller diameter
n	Rotation frequency
J	Propulsion coefficient
σ_n	Cavitation number
r_α	Phase volume fraction
u_i	Velocity component (m s ⁻¹)
\dot{S}_α	Phase mass transfer rate (Kg m ⁻³ s ⁻¹)
g_i	Gravity component (m s ⁻²)
P	Pressure (N m ⁻²)
\bar{u}_i	Average velocity component (m s ⁻¹)
u_i'	Fluctuating velocity component (m s ⁻¹)
k	Kinetic energy (m ² s ⁻²)
Ω	Vorticity
S	Shear Strain Rate
v_{in}	Inlet normal velocity
p_{out}	Outlet static pressure
Q	Q-criteria value
Q^*	Dimensionless Q-criteria value

Greek letters

ε	Turbulence dissipation rate (m ² s ⁻³)
ω	Turbulence frequency (s ⁻¹)
ρ_α	Phase density (Kg m ⁻³)
τ_{ij}	Stress tensor component (Kg m s ⁻²)
σ	Surface tension coefficient (m ³ s ⁻²)

Subscripts

m	Mixture
-----	---------

ACKNOWLEDGMENTS

Presented investigations have been supported by the German Ministry of Education and Research (BMBF) under grant number 03SX202A.

REFERENCES

- [1] Menter F.,2002, "CFD Best Practice Guidelines for CFD Code Validation for Reactor Safety Applications", ECORA Project, pp. 1-47.
- [2] Frank, T., Lifante, C., Rieck, K, 2007, „CFD Simulation of Cloud and Tip Vortex Cavitation on Hydrofoils”, *Proceedings of the International Conference on Multiphase Flow*. ICMF 07, Leipzig.

- [3] Lifante, C., Frank, T., Rieck, K, 2007, "Investigations of Pressure Fluctuations caused by Turbulent and Cavitating Flow around a P1356 Ship Propeller", *Proceedings of the ANSYS Conference & 25 CADFEM Users Meeting*. ACUM07. Dresden.
- [4] Lifante, C., Frank, T., Kuntz, M, 2007, „Extension and Validation of the CFX Cavitation Model for Sheet and Tip Vortex Cavitation on Hydrofoils”, *5th Joint FZR & ANSYS Workshop "Multiphase Flows: Simulation, Experiment and Application"*, Dresden.
- [5] Anschau, P. Mach, K-P., Rieck, K. 2007, „Stereo PIV measurements for CFD Validation“. *Proceedings of the ANSYS Conference & 25 CADFEM Users Meeting*. ACUM07. Dresden.
- [6] www.sensoren.de/drucksensoren.htm
- [7] ANSYS Inc., 2007, ICEM-CFD 12.0 "Users Manual"
- [8] ANSYS Inc., 2007, ANSYS CFX 12.0 "Users Manual".
- [9] Schneiders, R., Schindler, R., Weiler, F., 1996, "Generation of Hexahedral Element Meshes". *Proceedings of the 5th International Meshing Roundtable*, Pittsburgh, USA.
- [10] Menter F., 1994, "Two-Equation Eddy-Viscosity Turbulence Models for Engineering Applications", *AIAA Journal*, Vol. 32, No. 8, pp. 1598-1605.
- [11] Menter, F.R., Rumsey, C.L., 1994, "Assessment of Two-Equation Turbulence Models for Transonic Flows", *AIAA 94-2343*, Proc. 25th Fluid Dynamics Conference, Colorado Springs, Colorado, U.S.A.
- [12] Jones, W. P.; Launder, B. E., 1973, The Calculation of Low-Reynolds- Number Phenomena with a Two-Equation Model of Turbulence. *International Journal for Heat and Mass Transfer*, 16, 1119.
- [13] Wilcox, D.C., 1988, "Reassessment of the Scale-Determining Equation for Advanced Turbulence Models", *AIAA J.*, Vol. 26, S. 1299-1310
- [14] Wilcox, D.C., 2000, "Turbulence Modelling for CFD", DCW Industries
- [15] Spalart, P.R., Shur, M.L., 1997, „On the sensitization of turbulence models to rotation and curvature”, *Aerospace Science and Technology*, Vol. 1-5, S. 297-30
- [16] Langtry, R., Menter, F., 2005, "Transition Modeling for General Applications in Aeronautics", *AIAA*, paper 2005-522
- [17] Wilcox, D.C., 1986, "Multiscale model for turbulent flows", In *AIAA 24th Aerospace Sciences Meeting*. American Institute of Aeronautics and Astronautics,
- [18] Menter, F. Egorov, Y., 2005, "A Scale-Adaptive Simulation Model using Two-Equation Models", *AIAA Paper 2005-1095*, Reno/NV.